IVYSPRING INTERNATIONAL PUBLISHER

Theranostics

2012; 2(10):976-987. doi: 10.7150/thno.5116

Research Paper

Plasmonic Nanobubbles Rapidly Detect and Destroy Drug-Resistant Tumors

Ekaterina Y. Lukianova-Hleb[1], Xiaoyang Ren[2], Debra Townley[3], Xiangwei Wu[2], Michael E. Kupferman[4], Dmitri O. Lapotko[1,5]✉

1. Department of Biochemistry and Cell Biology, Rice University, Houston, TX;
2. Department of Cancer Prevention, UT MD Anderson Cancer Center, Houston, TX;
3. Department of Molecular and Cellular Biology, Baylor College of Medicine, Houston, TX;
4. Department of Head and Neck Surgery, UT MD Anderson Cancer Center, Houston, TX;
5. Department of Physics and Astronomy, Rice University, Houston, TX, USA.

✉ Corresponding author: dl5@rice.edu

Received: 2012.08.28; Accepted: 2012.09.22; Published: 2012.10.13

Abstract

The resistance of residual cancer cells after oncological resection to adjuvant chemoradiotherapies results in both high recurrence rates and high non-specific tissue toxicity, thus preventing the successful treatment of such cancers as head and neck squamous cell carcinoma (HNSCC). The patients' survival rate and quality of life therefore depend upon the efficacy, selectivity and low non-specific toxicity of the adjuvant treatment. We report a novel, theranostic *in vivo* technology that unites both the acoustic diagnostics and guided intracellular delivery of anti-tumor drug (liposome-encapsulated doxorubicin, Doxil) in one rapid process, namely a pulsed laser-activated plasmonic nanobubble (PNB). HNSCC-bearing mice were treated with gold nanoparticle conjugates, Doxil, and single near-infrared laser pulses of low energy. Tumor-specific clusters of gold nanoparticles (solid gold spheres) converted the optical pulses into localized PNBs. The acoustic signals of the PNB detected the tumor with high specificity and sensitivity. The mechanical impact of the PNB, co-localized with Doxil liposomes, selectively ejected the drug into the cytoplasm of cancer cells. Cancer cell-specific generation of PNBs and their intracellular co-localization with Doxil improved the *in vivo* therapeutic efficacy from 5-7% for administration of only Doxil or PNBs alone to 90% thus demonstrating the synergistic therapeutic effect of the PNB-based intracellular drug release. This mechanism also reduced the non-specific toxicity of Doxil below a detectable level and the treatment time to less than one minute. Thus PNBs combine highly sensitive diagnosis, overcome drug resistance and minimize non-specific toxicity in a single rapid theranostic procedure for intra-operative treatment.

Key words: plasmonic nanobubble, cancer cell,

INTRODUCTION

One of the major limitations of traditional treatments of cancers is the inability to surgically resect a tumor completely without having to remove large areas of normal tissue that serve critical functions. Residual tumor cells form the nidus for local recurrences and delayed metastases, which are seen commonly in head and neck, prostate and other cancers. Not only does this profoundly impact patients' overall survival, but also their quality of life, due to extensive treatment-related anatomic and functional alterations. The residual cancer cells at the surgical margins often show high resistance to local and sys-

temic adjuvant chemotherapy and radiotherapy [1], thus requiring toxic levels of these treatments. This is of particular concern in head and neck squamous cell carcinoma (HNSCC), the sixth most common cancer diagnosis worldwide, with an estimated 263,000 newly-diagnosed cases and over 128,000 deaths occurring yearly [2]. Hence, there is a critical need to develop novel diagnostic and therapeutic modalities that not only complement current therapies to enhance tumor control, but also simultaneously limit the treatment-related morbidity that ensues from treatment intensification, and can be applied as intra- or post-operative treatments.

Recently introduced approaches have employed nanoparticles (NPs) and external energies to develop putative tumor-targeting capabilities through drug delivery [3-20], hyperthermia [21-31] and photodynamic therapy [31-33]. However, the promises of these new modalities did not provide their fast translation from the lab to the clinic for the following reasons: (i) low NP targeting specificity, (ii) tumor cell heterogeneity, (iii) resistance of phenotypes [1, 3, 4] and (iv) NP or energy-delivery toxicities [20-29, 34-36]. Therefore, the development of novel technologies that will (a) selectively detect and eliminate drug-resistant residual cancer cells to prevent local and regional recurrence, (b) preserve the functionality of normal tissues and (c) reduce non-specific toxicity, is highly significant. In addition, an ability to unite both tumor detection and its treatment in one real-time intra-operative theranostic procedure will improve the principal limitations of cancer surgery cited above.

In order to overcome the limitations of the NP- and external energy-based medicine, we recently introduced a new class of threshold-activated cellular nano-agents, called plasmonic nanobubbles (PNBs). A PNB is a laser pulse-induced nanoscale explosive event that develops only if the energy (fluence) of laser pulse exceeds specific threshold of the evaporation of NP environment, a vapor nanobubble and not a NP, although it employs a gold NPs or their cluster to convert optical energy into heat for the evaporation of the liquid surrounding super-heated NP. The major difference that distinguishes PNBs from existing nano-agents is their on-demand threshold and transient nature, dynamic tunability and mechanical, not thermal, therapeutic mechanisms [37-40]. PNBs offer several unique oportunities that are not addressed by current methods (both traditional and those using various NPs and external energies). These are: (i) broad-spectrum efficacy against the major mechanisms of drug resistance; (ii) selectivity due to efficient discrimination of cancer from normal cells and (iii) multi-functionality of diagnosis (through optical and acoustic signals [38, 39, 41]) and guided cell level therapeutics [37-40, 42].

Based on the above, we hypothesized that the synergistic effect of PNBs coupled with low doses of traditional cytotoxic chemotherapies, gold NPs and optical energy would rapidly and selectively eliminate drug-resistant micro-tumors in a single pulse treatment (Figure 1). We further hypothesized that the acoustic detection of PNB will provide simultaneous diagnostic tumor imaging and guidance of drug delivery (Figure 1). Utilizing models of HNSCC, we studied the *in vitro* and *in vivo* PNB generation, detection and intracellular delivery of encapsulated drug (Doxil) with the focus on providing high diagnostic and therapeutic efficacy and reducing non-specific therapeutic toxicity and the treatment time in a single theranostic procedure.

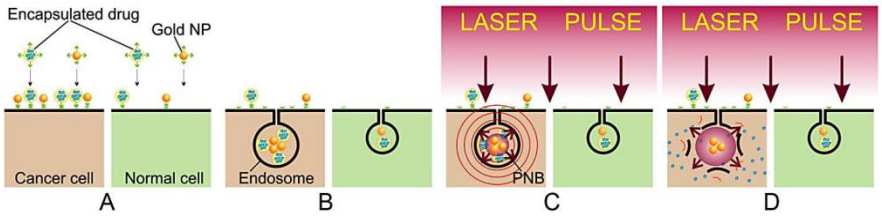

Figure 1. (**A**): Separate administration of gold NP conjugates and encapsulated drug; (**B**): cancer cell self-assembles mixed clusters of the drug carriers and gold NPs during receptor-mediated endocytosis; (**C**): diagnostic function is provided by the selective generation of PNB around the cluster of gold NPs with a single laser pulse and remote real-time detection of the acoustic response of the PNB; single gold NPs in normal (*green*) cells have a higher threshold of PNB generation and thus do not produce a PNB under a low level of laser pulse fluence; (**D**): selective therapeutic effect is provided by explosive localized disruption of drug carrier and endosome by PNB and the ejection of the drug (*blue dots*) into cytoplasm.

MATERIALS AND METHODS

PNB generation for drug delivery and diagnostics

To overcome drug resistance of HNSCC and to reduce non-specific toxicity of anti-tumor drug we applied active and HNSCC cell-specific delivery of encapsulated doxorubicin (Doxil) into the cytoplasm of HNSCC cells in order to create a high local concentration of the drug. Instead of the existing passive diffusion-based mechanisms, we employ the PNB-induced localized, mechanical ejection of the drug from liposome and from endosomes (Figure 1D). This is achieved by generating small intracellular PNBs (non-invasive on their own), co-localized with drug liposomes in the complex intracellular clusters. The key to this method is in the separate administration of Doxil (Doxorubicin encapsulated into 85 nm liposomes) at significantly reduced doses and the conjugates of gold NPs with C225 antibody (Erbitux) (Figure 1A). Solid gold spheres of 20 nm and 60 nm diameter, the most available and FDA-approved gold NPs, were employed because they showed high PNB generation efficacy under near-infrared (780 nm) pulsed optical excitation (Figure 4C). Gold NPs and Doxil are non-toxic even when they are internalized by the cells, including their non-specific uptake by normal cells (Figure 1B). The therapeutic mechanism is provided by two steps: (i) cancer cells selectively self-assemble large, complex clusters of gold NPs co-localized with drug liposomes (Figure 1B) through receptor-mediated endocytosis (while normal cells cannot accumulate so many gold NPs and build clusters of the same size as cancer cells); and (ii) the threshold generation of PNBs around gold NPs in these clusters with a single laser pulse at 780 nm, 70 ps (Figure 1C and D). Gold spheres efficiently generated PNBs with this short NIR laser pulse through our new method that employs the specific duration and low, safe fluence of the single laser pulse. These PNBs are small and therefore non-invasive alone [38, 40] (see also Figure 2C, 5D), but they simultaneously deliver two important functions. Their optical scattering and acoustic emission provide the remote and immediate detection of cancer cells (Figure 1C), and their mechanical, not thermal, impact immediately disrupts the liposome and endosome membranes and the pressure created by the expanding PNB ejects the drug into the cellular cytoplasm (Figure 1D). This fast (nanosecond) and localized (submicrometer) mechanism creates a high local intracellular concentration of the drug that is impossible to achieve through conventional slow delocalized diffusive processes of drug delivery. This overcomes most of the known mechanisms of drug resistance and, in addition, allows the reduction of the initial dose of the drug to a level that does not cause non-specific toxicity.

HNSCC models

We used multi drug-resistant HN31 squamous carcinoma cells (associated with head and neck cancers) expressing epidermal growth factor receptor (EGFR) and immortalized normal human oral kerotinocyte NOM9 cells. The co-culture of HN31 and NOM9 cells was treated with 60 nm gold NP-C225 conjugates using the clinically-validated C225 antibody against EGFR, the main molecular target in the treatment of HNSCC [43-45]. Cancer cells were identified among normal cells through the fluorescence of pre-transferred Green Fluorescent Protein (Figure 2).

In vitro Doxil and NP-C225 conjugates were separately administered to cells during 24 hours (Figure 1A) and were then washed off prior to laser treatment. Thus the cells were exposed only to the internalized drug during the follow up generation of PNBs. The concentration of Doxil was varied from the therapeutic dose of 100 μg/ml [46] down to 1μg/ml. Uptake of NPs and Doxil by living cells was assayed with a confocal microscopy (LSM-710) in the bright field, optical scattering and two fluorescent modes.

The *in vivo* model used mice with the same cancer cells. Tumors were xenografted with the HN31 cell lines as previously described [47]. All animals were monitored for tumor growth on a daily basis. When tumors reached 5-6 mm in diameter, gold NP-C225 conjugates were administered locally (intra-tumoral injection of 1 μl at $9x10^{12}$ NP/mL (0.8 μg/g) and systemically (intravenous injection in a tail vein of 200 μL at $4.5x10^{10}$ NP/mL (0.8 μg/g) at two diameters of NPs, 20 nm and 60 nm. Doxil was injected intratumorally at three-fold reduced dose of 1 mg/kg relative to the therapeutic dose [46]. Twenty-four hours after the injection of gold NP-C225 conjugated and the drug, laser treatment of the animals was performed. The laser beam was scanned across the surface of the tumor and normal tissue at the speed of 1 mm^2/s. The scan speed, beam diameter and pulse repetition rate (20 Hz) were synchronized in order to provide a single pulse exposure mode for each area of the tumor and tissue. Each treatment mode was applied to 3-5 animals. Animals were treated in accordance with the institutional guidelines and protocols of the University of Texas M. D. Anderson Cancer Center.

Detection of PNBs

PNBs were detected, imaged and measured through three independent methods that were em-

ployed simultaneously (Supplementary Material: Figure S1). Optical scattering was employed in the two methods of time-response and time-resolved imaging. The duration of the optical scattering time-response was measured as the lifetime of the PNB. Time-resolved scattering images were used to image the location of PNBs *in vitro*. Acoustic detection employed the generation of the pressure transients during the PNB expansion and collapse, complemented optical scattering detection, and, most importantly for the diagnostic application, provided the *in vivo* detection of PNBs in opaque tissue. The amplitude of acoustic response was used as the PNB metric and was correlated to the optically measured lifetime of PNB (Supplementary Material: Figure S2F).

Statistics

Two-tailed t-tests were used to compare PNB lifetimes, cell death and necrosis levels from control groups and treatment groups. Statistical analyses were performed with Origin software (OriginPro8, OriginLab Corporation, Northampton, MA). p values < 0.05 were considered statistically significant.

Other details of the experimental methods can be found in the Supplementary Material.

RESULTS

NP clustering and PNB generation and detection in cancer cells

The mechanism of the formation of mixed gold NP-drug carrier clusters and on-demand generation of PNBs around such clusters was studied in a co-culture of drug-resistant HNSCC cells and normal cells.

Selective formation of mixed intracellular clusters of gold NPs and Doxil. The NP clustering and co-localization with Doxil was analyzed with confocal microscopy in scattering (for gold NPs) and fluorescent (for Doxil that contains fluorescent doxorubicin) modes (Figure 2A). A co-culture of HN31 (HNSCC) and NOM9 (normal) cell was treated with C225 conjugates of solid gold 60 nm spheres and Doxil liposomes. The antibody C225 (Erbitux) was clinically proven to target the Epidermal Growth Factor Receptor (EGFR) in HNSCC [43-45] and provided intracellular clustering of gold NP-C225conjugates through the mechanism of EGFR-mediated endocytosis [38, 48, 49]. Individual HN31 cells were identified through the fluorescence of the transfected Green Fluorescent Protein (Supplementary Material: Figure S2A). Analysis of the confocal images of cancer cells revealed complex clusters with gold NPs (*blue* in Figure 2A) co-localized with Doxil (*red* in Figure 2A). Adjacent normal cells also showed occasional NPs due to their non-specific accumulation, but no large NP-Doxil clusters were detected in normal cells (Figure 2A). Thus the complex large NP-Doxil clusters were selectively self-assembled only by cancer cells during the separate administration of Doxil and gold NPs.

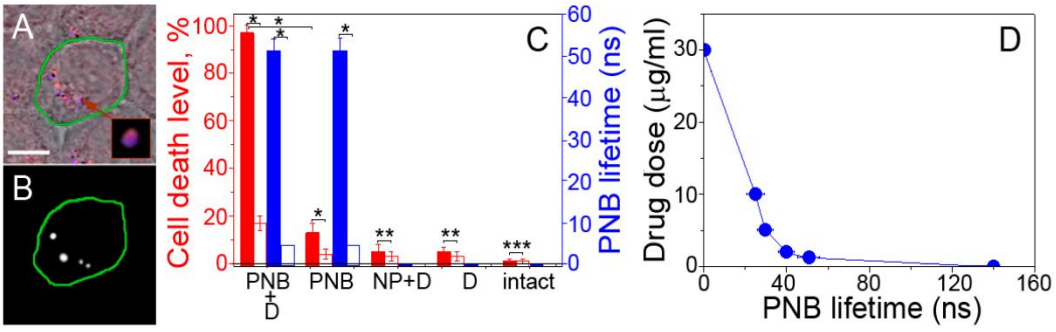

Figure 2. PNB-enhanced endosomal escape *in vitro*. (**A**): Confocal microscopy images of cancer (*green boarder*) and normal (*adjacent*) cells show NPs (*blue*) and Doxil (*red*) co-localized in the large mixed clusters (inset) only in cancer cell while adjacent normal cells show non-specific uptake of NPs and Doxil (scale bar is 5 μm); (**B**): time-resolved optical scattering image of the same sample shows PNBs selectively generated with a broad single laser pulse (780 nm, 70 ps, 40 mJ/cm^2) only in cancer cell and their co-localization with NP-Doxil clusters; (**C**): PNB lifetime (*blue bars*) and cell death level (*red bars*) measured in 72 h after laser treatment for cancer (*solid bars*) and normal (*hollow bars*) cells after the application of several treatment modes (PNB+D: single laser pulse, NPs and Doxil, PNB: single laser pulse and NPs; NP+D: NPs and Doxil (* $p < 0.001$, ** $p<0.05$, *** $p > 0.05$); D: Doxil, intact: non-treated cells); (**D**): DL50 dose for cancer cells as function of drug dose and PNB lifetime.

Generation and detection of PNBs in individual cells. We next determined the conditions of the PNB generation in the complex NP-Doxil clusters in cells. PNBs were generated by exposing the co-culture of HN31 and NOM9 cells to single near-infrared laser pulses (70 ps, 780 nm) of broad diameter (that provided the simultaneous irradiation of cancer and normal cells) and varying laser fluence (the energy per unit of square) in the range of 10-100 mJ/cm^2 (Supplementary Material: Figure S1). In this work we applied for the first time the safest combination of FDA-approved solid gold spheres and near-infrared laser radiation in a low dose that provides the deepest tissue penetration and the minimal bio-damage [50]. Optical scattering time-resolved imaging (Figure 2B and Supplementary Material: Figure S2) and optical scattering time-responses (Supplementary Material: Figure S2) were obtained for individual cancer and normal cells simultaneously with the excitation laser pulses and were employed to image and quantify PNBs in the irradiated cells.

Both images (Figure 2B and Supplementary Material: Figure S2) and time-responses (Supplementary Material: Figure S2) showed the cancer cell-specific generation of PNBs while normal by-stander cells in the co-culture produced no or very small PNBs in a wide range of laser pulse fluences (Figure 2B and Supplementary Material: Figure S2E). This demonstrated the selectivity of the cluster-threshold mechanism of PNB generation. The comparison of the optical scattering images of PNBs (Figure 2B) and NP-Doxil clusters (Figure 2A) revealed their good co-localization in cells. Thus the mixed NP-Doxil clusters acted as PNB sources and the mechanical impact of PNBs was co-localized to Doxil liposomes. In this experiment PNBs provided optical detection of cancer cells with high specificity and sensitivity.

The mechanism of drug delivery with PNBs

The mechanism of intracellular delivery and on-demand release of an encapsulated drug (doxorubicin in Doxil liposomes) was studied in the same co-culture of HN31 and NOM9 cells.

Therapeutic effect of PNBs in vitro was measured 72 hours after a single pulse laser treatment as the level of cancer cell death in several different treatment modes (Figure 2C). We correlated the size of PNBs (measured by their lifetimes, obtained as the duration of time-responses of individual cells, Supplementary Material: Figure S2) to their therapeutic effect. Relatively small PNBs of 20-90 ns lifetime showed the low therapeutic efficacy (low death level for cancer cells) and the low non-specific toxicity (low death level for normal cells) when used alone (Figure 2C). Earlier we found that only large PNBs with a lifetime > 130 ns mechanically kill the cells [38, 39].

Synergistic effect of PNB and Doxil. Direct exposure of cells to Doxil and gold NPs without laser pulses had a limited effect on cancer cells due to their drug resistance coupled with a relatively low dose of Doxil (5 μg/ml, 20-fold lower than the effective therapeutic dose [46]). Such a low dose of the drug reduced non-specific toxicity, as we observed minimal damage to normal cells (Figure 2C). However, when PNBs were generated in the mixed NP-Doxil clusters, the cell death level increased by 30-fold among cancer cells (relative to the drug alone mode) but remained relatively low among normal cells where no PNBs were generated (Figure 2C). A quantitative analysis of the DL50 doses (the doses that caused 50% cell death level) for cancer cells as a function of the Doxil dose and PNB lifetime revealed the synergistic effect of the joint action of PNBs and Doxil (Figure 2D). The optimal PNB-Doxil combination corresponded to non-invasive PNBs of 51±7 ns lifetime (when used alone without the drug) and non-toxic doses of Doxil of 3 μg/ml (when used alone without the PNB).

This selective and efficient therapeutic effect was achieved due to the localized, active, mechanical release (ejection) of the drug from liposomes and endosomes (Figure 1D) that were disrupted by an expanding co-localized PNB. This process took tens of nanoseconds and required a single laser pulse of a low dose to provide the selective intracellular release of the drug only in cancer cells. We termed this mechanism, a PNB-enhanced endosome escape. Normal cells did not develop PNBs under identical laser and NP treatment and thus the Doxil liposomes non-specifically taken by normal cells (Figure 2A) were not disrupted by PNBs and did not release the drug (Figure 2C). Unique to this technology, PNBs provided the optical detection of cancer cells and their selective destruction in a single, fast theranostic procedure.

NP targeting, PNB generation and detection in HNSCC tumor *in vivo*

In order to translate the achieved result *in vivo* and to address the impact of tissue on the propagation of light and NPs, we first studied the delivery of NPs, laser radiation and the generation and detection of PNBs in a xenograft mouse model of HNSCC that used the same cancer cell line, HN31.

NP delivery and clustering in vivo. The formation of NP clusters in the tumor was imaged and quanti-

fied by using TEM microscopy and the PNB generation in the tumor slices. NP-C225 conjugates of solid gold 60 nm spheres were administered locally (intra-tumoral injection of 1 µl at $9x10^{12}$ NP/mL (0.8 µg/g) and systemically (intravenous injection in a tail vein of 200 µL at $4.5x10^{10}$ NP/mL (0.8 µg/g) at two diameters of NPs, 20 nm and 60 nm. In 24 hours after systemic administering 60 nm gold NP-C225, TEM analysis of the tumor and adjacent normal muscle tissue showed large clusters of gold NPs (an average size 297±135 nm) only in the tumor (Figure 3A) while non-specific uptake resulted in occasional single NPs in normal tissue (an average size close to that of a single NP, 64±15 nm, Figure 3B). Thus, despite a non-specific uptake of single gold NPs by normal tissues the sources of PNBs, larger NP clusters, were observed only in tumors and not in normal tissues.

Selectivity of PNB generation in tumor. Next, gold NP clusters were analyzed as PNB sources in tumor slices. Each individual cell in a slice was identically exposed to a single laser pulse and the PNB lifetimes were obtained for cancer (fluorescently-identified) and normal cells in a similar way to the above *in vitro* experiment (Supplementary Material: Figure S2C). At the fluence of 40 mJ/cm^2 single pulse excitation resulted in the generation of PNBs only in cancer cells while normal cells did not generate PNBs under such a low fluence level (Figure 3C). This result indicated that tumor-specific gold NP clusters (not present in normal cells and tissues) provided selective generation of PNBs only in tumor cells. The mechanism of such high selectivity is based on the dependence of the PNB generation threshold upon the size of the NP or its cluster: the threshold fluence decreases with the cluster size [41, 42, 49, 62].The level of laser pulse fluence applied was below the PNB generation threshold for single NPs but above the PNB generation threshold for large NP clusters. These results correlated well to those obtained previously *in vitro* (compare Figure 3C to Figure 2C) and demonstrated selective formation of NP clusters and PNB generation only in tumor while the non-specifically taken gold NPs in normal tissue did not form clusters and therefore were unable to generate PNBs.

Detection of PNBs in vivo in opaque tissue. Due to the limited optical transparence of real tissue in animals we replaced the optical detection of PNBs with the acoustic method (Figure 4A). Briefly, the expansion and collapse of a PNB produces pressure pulses (Figure 1C, red) that can be remotely detected in opaque tissue in animals with an ultrasound detector as PNB-specific acoustic time-responses (Figure 4B). The amplitude of the acoustic response of a PNB was found to be almost linearly proportional to the optically measured lifetime of the same PNB (Supplementary Material: Figure S2F). Thus we employed the acoustic signal amplitude as an *in vivo* metric of PNB.

Near-infrared pulsed excitation of PNBs in tumor. Next, in order to optimize the laser wavelength for the near-infrared excitation the acoustic amplitudes of PNBs were obtained as the spectra of the excitation laser wavelength in tumor and normal tissue in animals that received intravenous gold NP-C225 conjugates and for a intact tumor in animals that did not receive any gold NPs (Figure 4C). Spectrum of the tumor in the NP-treated animal showed a 3 nm wide peak at 780 nm. Other NIR wavelengths returned much lower signals comparable to the background level. The normal tissue of the NP-treated animal showed very small acoustic signals that were also comparable to the background level, while intact tumor returned zero signals under identical optical excitation (Figure 4C). We concluded that the detected acoustic signals of the NP-treated tumor were associated with gold NP clusters that were selectively formed in the tumor cells as we found previously (Figure 3A). We therefore employed the near-infrared wavelength of 780 nm for the experiments *in vivo*.

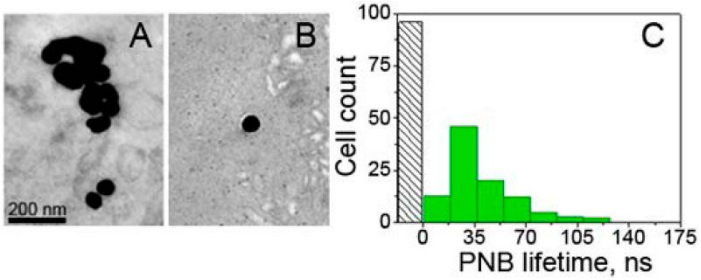

Figure 3. NP-C225, solid gold 60 nm spheres conjugates in HNSCC-bearing mouse: transmission electron microscopy image of a tumor (**A**) and adjacent muscle tissue (**B**) in 24 h after systemic injection of NP-C225 to mouse. (**C**): Histogram of the PNB lifetime obtained for individual cells in slices of tumor for cancer (*green*) and normal (*grey*) cells after being extracted from mice in 24 hours after systemic administering of NP-C225.

Figure 4. PNBs in HNSCC-bearing mouse. (**A**): Functional diagram of the experimental set up, optical fiber delivers short laser pulse through the surface of the tissue, PNBs are detected with ultrasound detector, which signals, the scan of the fiber and laser pulse generation are controlled by computer program; (**B**): acoustic responses to single laser pulses (70ps, 780 nm, 40 mJ/cm^2) obtained from a tumor (*green*) and adjacent muscle (*black*) in mouse systemically treated with 60 nm solid gold sphere conjugates, NP-C225; (**C**): Spectrum of PNB amplitudes of acoustic responses obtained from a squamous cell carcinoma tumor (*solid green*) and normal tissue (*hollow black circles*) of a mouse systemically treated with C225-conjugated 60 nm gold spheres, tumor in intact animal (*solid black squares*) and (40 mJ/cm^2); (**D**): Ddependence of the amplitudes of acoustic responses upon laser pulse fluence (energy per square unit) for the same animals obtained from the tumor (*green*) and adjacent muscle (*black*) (* $p < 0.001$); (**E**): acoustic amplitudes obtained during the scans of the tumor, muscle and blood of NP-treated animals and of a tumor of an intact animal (* $p < 0.001$); (**F**): dependence of PNB lifetime (*blue*, optical response obtained from individual tumor cells *in vitro*) and the acoustic amplitude of PNB (*green*, acoustic response obtained from a tumor in animal) as function of NP size (20 nm and 60 nm) and *in vivo* administration route (local intra-tumor injection and intra-venous injection) under identical laser excitation (single pulse,70 ps,780 nm, 40 mJ/cm^2).

Real-time detection of the tumor with acoustic signals of PNBs. The specificity and sensitivity of the tumor detection were studied through the amplitude of acoustic signal of PNBs that was measured as function of tissue type and of the laser excitation fluence. The amplitude of PNB signal increased with the fluence of the excitation laser pulse (Figure 4D). It should be noted that just a single laser pulse was required to detect a tumor-specific acoustic signal. The duration of this diagnostic process was limited by the speed of

the ultrasound detector and was below one millisecond.

During the laser scans of a tumor and normal adjacent tissue in the NP-treated animals, the detectable acoustic signal of the PNBs was observed only for the tumor and not for normal muscle tissue and blood (Figure 4D). Tumors in intact animals (that did not receive gold NPs) did not yield any detectable acoustic signal under the identical fluence of laser pulse (Figure 4D). Therefore, the optical fluence of 40 mJ/cm^2 was below the bubble generation threshold in blood and other normal tissues for the employed NIR wavelength (780 nm) and duration (70 ps) of laser pulse. The results demonstrated high sensitivity, specificity, safety and speed of tumor detection in a single near-infrared laser pulse procedure.

Optimization of the NP size and delivery route for PNB generation in vivo. In addition, we analyzed the influence of the NP diameter and delivery route on PNBs generation *in vitro* and *in vivo*. The intravenous systemic delivery of NPs resulted in larger PNBs compared to local intra-tumor injection of the same NPs under identical optical excitation (Figure 4E). In both cases the NP-C225 conjugates were administered 24 hour prior to the laser treatment. Larger 60 nm NPs generated larger PNBs compared to smaller 20 nm NPs both *in vivo* and *in vitro* conditions (Figure 4F). We therefore used systemic intravenous delivery of solid gold 60 nm sphere conjugates, NP-C225, for the next, therapeutic stage.

PNB therapeutics of HNSCC tumor *in vivo*

The therapeutic mode of PNBs employed both the above methods of generation and detection of PNBs *in vivo* and of PNB-enhanced endosome escape intracellular delivery of the encapsulated drug. We next determined the therapeutic efficacy of tumor-targeted PNBs and Doxil in a mouse model of HNSCC.

In vivo administration of NPs, Doxil and laser radiation for cancer therapeutics. We separately administered Doxil- and gold 60 nm NP-C225 conjugates to an HNSCC bearing mouse. Doxil was administered locally at the concentration of 1mg/kg, 3-fold lower than therapeutic concentration [46]. NP-C225 conjugates were administered intravenously simultaneously with Doxil at the concentration of 4.5x10^{10} NP/mL (200 µl). After 24 hours, one-half of the tumor and the adjacent normal tissue were scanned with single laser pulses at 20Hz while the intact part of the tumor was used as the non-irradiated control. We applied the single laser pulse irradiation with the same parameters as those established earlier *in vitro*, 780 nm, 70 ps, 40 mJ/cm^2, and increased the laser beam diameter to 0.25 mm in order to improve the tissue penetration depth [50]. The part of animal surface with the tumor and normal tissue was scanned with the laser beam at the rate 1 mm^2/s. Real-time acoustic monitoring showed the PNB signals of 36± 3 mV amplitude for the tumor (Figure 5D) and 0 mV for the adjacent muscle tissue. This result approximated the previous *in vivo* diagnostic experiment (Figure 4B and D) and confirmed the tumor-specific generation of PNBs in therapeutic mode.

Therapeutic effects of PNBs and Doxil. Next, we analyzed the effect of several treatment combinations for tumor and for adjacent normal muscle tissue: (i) single laser pulse + NP + Doxil, (ii) single laser pulse + NP (PNBs alone, similar to the diagnostic mode), (iii) NP + Doxil (evaluation of the toxicity of NPs and drug), (iv) Doxil (analog of standard chemotherapy at the reduced dose) and (v) intact tumor or muscle. After 72 hours, the tumor and normal tissue were harvested and the relative level of necrosis was analyzed with a standard histopathological technique (see Supplementary Material). The analysis of the level of necrosis in the tumor (Figure 5A-C) showed a high damage zone only for the combination laser pulse + NP + Doxil (Figure 5A and D) that was associated with the generation of small PNBs. This result corresponded to *in vitro* case of the co-localized PNBs and Doxil (Figure 2C). The therapeutic effects of the PNBs or Doxil alone were low, less than 7% each (Figure 5B and D), meaning that only small non-invasive PNBs were generated. This non-invasive nature of PNBs alone was in line with the corresponding *in vitro* results that also showed low PNB-induced cell death (Figure 2C). The toxic effect of NPs was also low (Figure 5C and D). Therefore, the single low dose of Doxil applied coupled with the drug resistant nature of the HNSCC tumor resulted in the low therapeutic efficacy. In contrast, the joint action of PNBs and Doxil resulted in the synergistic enhancement of the necrosis level up to 80-92%, while the additive effects of PNBs alone and Doxil alone did not exceed the necrosis level of 13% (Figure 5D). This demonstrates how PNB-enhanced endosomal escape mechanism overcomes the drug resistance of HNSCC even under the low dose of the drug. In addition, the level of necrosis correlated well to the acoustic amplitude of PNBs in drug-treated animals (Figure 5D) thus allowing the real-time guidance of the therapeutic efficacy of PNBs during the laser scan.

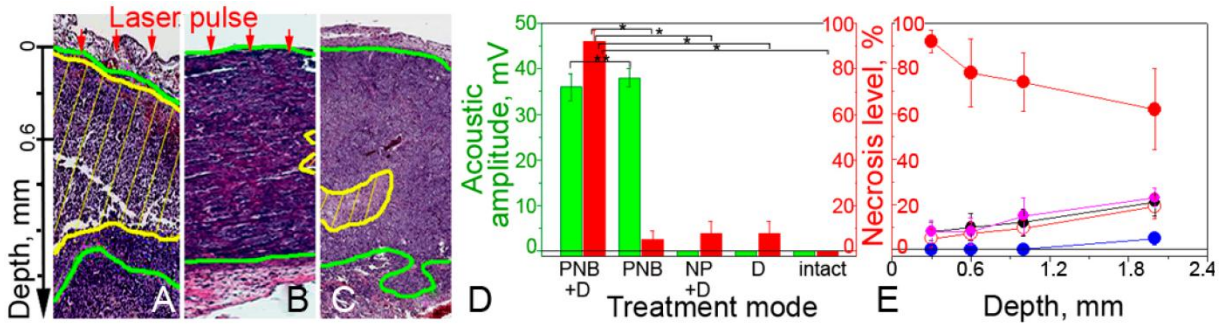

Figure 5. PNB therapeutics of HNSCC tumor in mouse. Tumor depth profiles in (**A-C**) show tumor (*green*) and necrotic tumor (*yellow*) for the treatment modes: (**A, E,** *solid red*): PNB+D: small PNBs (40 mJ/cm^2 @780 nm, 70 ps, single pulse, NP: gold 60 nm spheres conjugated to C225) and Doxil (1 mg/kg); (**B, E,** *hollow red*): PNBs alone; (**C**, **E,** *hollow black*): Doxil+NP; (**D**): Level of necrosis (*red bars*) at 0.3 mm depth and acoustic signals of PNBs (*green bars*) for the listed treatment modes ($p < 0.001$, ** $p > 0.05$). (**E**): Dependence of the level of necrosis in tumor upon tissue depth (PNB+D: *solid red*, PNB: *hollow red*, NP+D: *hollow black*, D: *magenta*, intact tumor: *blue*).

Correlation of in vitro and in vivo results and the PNB therapeutic mechanism. A comparison of the corresponding treatment modes *in vivo* and *in vitro* (Figure 2C vs Figure 5D) demonstrated the high similarity of the therapeutic effects in both models, thus confirming the earlier established therapeutic mechanism of PNB-enhanced endosomal escape of the drug from liposomes and endosomes (Figure 1D). Regardless of the mechanism of drug resistance, the cancer cell failed to protect itself from the mechanical explosive action of PNBs that ejected the drug into cellular cytoplasm. The nanosecond speed of this process was much higher than traditional diffusion-based release processes. Such fast release of the drug resulted in its high local intracellular concentration that was sufficient to kill drug-resistant cells after a single administration of a 3-fold reduced dose of Doxil. This, in turn, reduced the treatment time from up to a week [46] to less than 1 minute of laser scan.

Reduction of non-specific toxicity. As a result of the reduction in the drug, NP and optical doses, we observed very low non-specific toxicity. The levels of necrosis in normal tissue under an identical treatment combination (NP-C225 + Doxil + single laser pulse) were found to be 0 %, even despite non-specific uptake of NPs and the drug by normal cells and tissues. The threshold mechanism of PNBs prevented their generation in normal tissue (Figure 4C-E) and thus prevented the non-specific release of the drug in normal tissue. This demonstrated the high safety and selectivity of PNB therapeutics (see also the Discussion).

Penetration depth of the PNB treatment. In order to study the effect of the optical attenuation by the tumor we measured the level of necrosis level as a function of the tissue depth for all treatment modes (Figure 5E). The laser-NP-Doxil mode demonstrated high therapeutic efficacy (70-92%), up to 1.5-1.8 mm depth for the laser beam of 0.25 mm diameter. This was achieved by using the near-infrared wavelength (780 nm) that previously was shown to provide the maximal penetration depth and minimal phototoxicity on a tissue [50]. Since the penetration depth of laser radiation increases with the diameter of the laser beam [50] this parameter can be further improved by using broader laser beam.

To summarize the therapeutic studies *in vivo*, the application of small non-invasive PNBs for intracellular release of the low doses of encapsulated drug allowed us to overcome drug resistance and to reduce non-specific toxicity and treatment time.

DISCUSSION

Mechanism of PNB therapeutics versus current therapeutic mechanisms

Our results demonstrated simultaneous ability of PNBs to deliver high sensitive diagnosis and selective, efficient and localized therapeutics in a single laser pulse theranostic procedure. The therapeutic mechanism of PNBs is based on active intracellular drug delivery through rapid mechanical, non thermal, disruption of drug carriers and endosomes and localized ejection of drug into cytoplasm (Figure 1D). This mechanism is distinct from the existing drug delivery mechanisms that are slow or non-specific. Current approaches for *in vivo* drug delivery, direct or enhanced by hyperthermia or photodynamic therapy employ various NPs [3, 8, 9, 13, 14], external energies [15, 17, 18, 26-31] or their combinations [11, 12, 20, 21, 26, 31-33]. However, their efficacy is limited by the slow diffusive nature of the drug release, while non-specific uptake of NPs or the non-specific nature of the external energy-stimulated release increase required doses of drugs and NPs and cause significant non-specific toxicity.

There are also well-established delivery methods that employ cavitation bubbles as ultrasound- or optically-induced events [17, 18, 34-36, 51, 52] or nanobubbles as particles [53-58]. Similar to the previously discussed methods, these "bubble" methods have a non-specific release mechanism, generate large bubbles that cannot discriminate cancer from normal cells and increase non-specific toxicity. Furthermore, an ultrasound cannot be applied as a single short (< 1 ms) pulse.

In contrast, PNBs reduced the NP dose by 2-4 orders of magnitude compared to the photothermal therapies [21, 25, 27, 28, 30, 31] optical energy dose by 10^{1-4} fold compared to photothermal drug delivery [11, 12] and photodynamic therapies [31-33] and drug dose by > 3 fold compared to standard chemotherapy [46]. Most of all, PNBs provided a single cell selectivity of the therapeutics and spared even adjacent normal cells.

Mechanism of PNB diagnostics versus current diagnostic mechanisms

The diagnostic part of PNB theranostics is technically close to photoacoustic methods [59], but PNBs provide higher sensitivity and specificity of tumor detection compared to broadly used gold NPs as photoacoustic probes. Conventional photoacoustics employs acoustic emission from all NPs, instead of cancer cell-specific generation of PNBs only around NP clusters (Figure 1C) as can be seen by comparing Figure 3 and Figure 4B. Under identical optical excitation, PNBs emit stronger pressure pulses compared to those emitted by gold NPs [60]. This explains the high specificity of PNB signals as shown in Figure 4B and Figure 4C and the high sensitivity that allows to detect even single tumor cells among normal ones [38]. Thus the PNB method provided high sensitivity, specificity and speed of tumor detection in a single near-infrared laser pulse procedure under relatively low optical fluence of 40 mJ/cm^2, which is within the medical safety limits for laser radiation [61] and with the safest solid gold spheres.

Advantages of using PNBs as transient events instead of nano-materials with pre-determined properties

The results reported above were achieved due to the novel biophysical properties of PNB's: (i) explosive nano-event whose mechanical, not thermal, action rapidly creates a high intracellular concentration of the released drug (Figure 1); (ii) ability to scatter the light and to emit a pressure pulse makes it a sensitive cellular diagnostic probe [38, 62]; (iii) the cluster-threshold mechanism of PNBs overcomes non-specific uptake of gold NPs by normal cells because the PNB generation threshold is minimal for large clusters of NPs self-assembled by cancer cells [38, 40, 62]; (iv) a single NP cluster of 5-50 NPs per cell and a single laser pulse are sufficient for detecting and elimination the cancer cells with single PNB thus substantially reducing the NP and laser energy doses; (v) therapeutic and diagnostic functions of PNBs can be activated simultaneously in a single pulse procedure [39, 63]; (vi) a PNB can be generated with FDA-approved gold spheres and a single near-infrared laser pulse of low dose and the maximal tissue penetration depth [50], thus eliminating the need in specially-engineered near-infrared NPs (such as nanorods and other NPs) and in prolonged optical excitation.

Translational potential of PNBs

The major limitations of the PNB method are associated with the limited penetration of light and gold NPs into heterogeneous tumors and with phototoxicity. The energy of commercial lasers allows an increase in the diameter of the laser beam of up to 3-4 mm and thus to achieve 5-7 mm range of tissue depth [50] and 100 mm^2/s scan speed. Both metrics match the needs of intra-operative treatment of residual disease. The optical dose if near-infrared laser radiation required for PNB generation is relatively low 10-40 mJ/cm^2, 4-6 orders of magnitude lower than those employed in previously reported *in vivo* studies of photothermal hyperthermia with gold NPs (3 - 72 x10^2 J/cm^2) [11, 12, 25, 27, 28]. Such a reduction in optical dose was achieved by using a single pulse of low fluence instead of prolonged, continuous irradiation. In our method, the optical dose becomes equal to the pulse fluence and is comparable to the established laser safety limits of 30-50 mJ/cm^2 for pulsed laser radiation [46]. Using off-resonant near-infrared excitation of FDA-approved solid gold spheres reduces the laser-induced NP temperature and, therefore, the thermal damage to NPs and to surrounding tissues. The combination of the efficacy, cell selectivity, safety, single pulse speed and multi-functionality of PNB theranostics demonstrated in our experiments have not been achieved to date *in vivo* with any current technologies. This all demonstrates translational potential of PNBs for the intra-operative treatment of surgical bed for monitoring and eliminating residual disease in real time.

CONCLUSIONS

We demonstrated for the first time *in vivo* the novel concept of PNB theranostics that enables diagnosis through the acoustic detection of the PNBs and

the simultaneous efficient treatment of drug-resistant tumors through the PNB-enhanced endosomal escape mechanism of intracellular drug delivery in a single laser pulse procedure:

1. The tumor-preferred clustering of gold nanoparticle conjugates, coupled with the threshold mechanism of PNB generation provided the cell level specificity of tumor detection and elimination.

2. Plasmonic nanobubbles increased the therapeutic efficacy of the standard drug by more than 10-fold compared to chemotherapy alone (Doxil @ 1 mg/kg), and eliminated > 80% of the drug-resistant HNSCC tumor within 1 mm of tissue depth in a fast single treatment.

3. Cumulated non-specific toxicity of the drug, gold nanoparticles and laser radiation was reduced below a detectable level.

4. The treatment time was reduced to less than one min for a tumor of five mm size by non-invasively scanning single near-infrared laser pulses (780 nm, 70 ps) at the safe optical dose of 40 mJ/cm^2.

By using the safest and commercially available gold NPs, solid spheres, a low dose of near-infrared single laser pulse and standard encapsulated drugs (not linked to NPs), PNB technology can be applied for local and real-time adjuvant treatment of poorly-detectable and curable residual drug-resistant micro-tumors during or immediately after surgery. The universal mechanism of PNB technology allows its extension to many cancers and other pathologies that require precise local treatment and thus may complement existing surgical and chemotherapeutic approaches.

SUPPLEMENTARY MATERIAL

Supplementary Methods, Fig.S1-S3.
http://www.thno.org/v02p0976s1.pdf

ACKNOWLEDGEMENTS

This work was partially supported by National Institute of Health, grant R01GM094816. Authors thank Shaoyi Huang and Jinqiao Zhang of MD Anderson Cancer Center (Houston, TX) for their technical help with the animal experiments and Hannie and Glen Ford of BioAssayWork, LLC (Jamsville, MD) for their help with conjugation of gold NPs.

Competing Interests

The authors disclose no potential conflicts of interest.

References

1. Jemal A, Siegel R, Xu J, Ward E. Cancer statistics. *CA: Cancer J Clin.* 2009;60:277-300.
2. Jemal A, Bray F, Center MM, Ferlay J, Ward E, Forman D. Global cancer statistics. *CA: A Cancer J Clin*. 2011;61:69-90.
3. Cho K, Wang X, Nie S, Chen ZG, Shin DM. Therapeutic nanoparticles for drug delivery in cancer. *Clin Cancer Res.* 2008;14:1310-6.
4. Peer D, Karp JM, Hong S, Farokhzad OC, Margalit R, Langer R. Nanocarriers as An emerging platform for cancer therapy. *Nat Nanotechnol* 2007;2:751-60.
5. Kim B, Han G, Toley BJ, Kim CK, Rotello VM, Forbes NS. Tuning payload delivery in tumour cylindroids using gold nanoparticles. *Nat Nanotechnol*. 2010;5:465-72.
6. Pissuwan D, Niidome T, Cortie MB. The forthcoming applications of gold nanoparticles in drug and gene delivery systems. *J Control Release* 2011;149:65-71.
7. Braun GB, Pallaoro A, Wu G, Missirlis D, Zasadzinski JA, Tirrell M, *et al.* Laser-activated gene silencing via gold nanoshell-siRNA conjugates. *ACS Nano*. 2009;3:2007-15.
8. Biswas S, Dodwadkar NS, Deshpande PP, Torchilin VP. Liposomes loaded with paclitaxel and modified with novel triphenylphosphonium-PEG-PE conjugate possess low toxicity, target mitochondria and demonstrate enhanced antitumor effects *in vitro* and *in vivo*. *J Control Release.* 2012;159:393-402.
9. Woo HN, Chung HK, Ju EJ, Jung J, Kang HW, Lee SW, *et al*. Preclinical evaluation of injectable sirolimus formulated with polymeric nanoparticle for cancer therapy. *Int J Nanomedicine*. 2012;7:2197-208.
10. Koning GA, Eggermont AM, Lindner LH, Ten Hagen TL. Hyperthermia and thermosensitive liposomes for improved delivery of chemotherapeutic drugs to solid tumors. *Pharm Res.* 2010;27:1750-4.
11. Agarwal A, Mackey MA, El-Sayed MA, Bellamkonda RV. Remote triggered release of doxorubicin in tumors by synergistic application of thermosensitive liposomes and gold nanorods. *ACS Nano.* 2011;5:4919-26.
12. Park JH, von Maltzahn G, Ong LL, Centrone A, Hatton TA, Ruoslahti E, *et al.* Cooperative nanoparticles for tumor detection and photothermally triggered drug delivery. *Adv Mater.* 2010;22:880-5.
13. Stathopoulos GP, Antoniou D, Dimitroulis J, Michalopoulou P, Bastas A, Marosis K, *et al.* Liposomal cisplatin combined with paclitaxel versus cisplatin and paclitaxel in non-small-cell lung cancer: a randomized phase III multicenter trial. *Ann Oncol.* 2010;21:2227-32.
14. Zhang F, Zhu L, Liu G, Hida N, Lu G, Eden HS, *et al.* Multimodality imaging of tumor response to Doxil. *Theranostics*. 2011;1:302-9.
15. Kost J, Leong K, Langer R. Ultrasound-enhanced polymer degradation and release of incorporated substances. *Proc Natl Acad Sci U S A* 1989;86:7663-6.
16. McCarthy MJ, Soong DS, Edelman ER. Control of drug release from polymer matrices impregnated with magnetic beads - a proposed mechanism and model for enhanced release. *J Control Release.* 1984;1:143-7.
17. Husseini GA, Pitt WG. The use of ultrasound and micelles in cancer treatment. *J Nanosci Nanotechnol* 2008;8:2205-15.
18. Rapoport N. Ultrasound-mediated micellar drug delivery. *Int J Hyperthermia*. 2012;28: 374-85.
19. Shukla R, Chanda N, Zambre A, Upendran A, Katti K, Kulkarni RR, *et al.* Laminin receptor specific therapeutic gold nanoparticles (^{198}AuNP-EGCg) show efficacy in treating prostate cancer. *Proc Natl Acad Sci U S A* 2012;109:12426-31.
20. Yuan H, Fales AM, Vo-Dinh T. TAT peptide-functionalized gold nanostars: enhanced intracellular delivery and efficient nir photothermal therapy using ultralow irradiance. *J Am Chem Soc.* 2012;134:11358−61.
21. Huang HC, Yang Y, Nanda A, Koria P, Rege K. Synergistic administration of photothermal therapy and chemotherapy to cancer cells using polypeptide-based degradable plasmonic matrices. *Nanomedicine* 2011;6:459–73.
22. Pitsillides CM, Joe EK, Wei X, Anderson RR, Lin CP. Selective cell targeting with light-absorbing microparticles and nanoparticles. *Biophys J.* 2003;84:4023-32.
23. Cherukuri P, Glazer ES, Curley SA. Targeted hyperthermia using metal nanoparticles. *Adv Drug Deliver Rev.* 2010;62:339-45.
24. Huff TB, Tong L, Zhao Y, Hansen MN, Cheng JX, Wei A. Hyperthermic effects of gold nanorods on tumor cells. *Nanomedicine (Lond).* 2007;2:125-32.
25. Dickerson EB, Dreaden EC, Huang X, El-Sayed I, Chu H, Pushpanketh S, *at el.* gold nanorod assisted near-infrared plasmonic photothermal therapy (PPTT) of squamous cell carcinoma in mice. *Cancer Lett.* 2008;269:57–66.
26. Gilstrap K, Hu X, Lu X, He X. Nanotechnology for energy-based cancer therapies. *Am J Cancer Res.* 2011;1:508-20.

27. Choi WI, Kim JY, Kang C, Byeon CC, Kim YH, Tae G. Tumor regression in vivo by photothermal therapy based on gold-nanorod-loaded, functional nanocarriers. *ACS Nano*. 2011;5:1995-2003.
28. Li Z, Huang P, Zhang X, Lin J, Yang S, Liu B, *et al.* RGD-conjugated dendrimer-modified gold nanorods for in vivo tumor targeting and photothermal therapy. *Mol Pharm*. 2010;7:94-104.
29. Gobin AM, O'Neal DP, Watkins DM, Halas NJ, Drezek RA, West JL. Near infrared laser-tissue welding using nanoshells as an exogenous absorber. *Lasers Surg Med*. 2005;37:123-9.
30. Gormley AJ, Larson N, Sadekar S, Robinson R, Ray A, Ghandehari H. Guided delivery of polymer therapeutics using plasmonic photothermal therapy. *Nano Today*. 2012;7:158-67.
31. Jang B, Park JY, Tung CH, Kim IH, Choi Y. Gold nanorod-photosensitizer complex for near-infrared fluorescence imaging and photodynamic/photothermal therapy in vivo. *ACS Nano*. 2011;5:1086-94.
32. Záruba K, Králová J, Rezanka P, Poucková P, Veverková L, Král V. Modified porphyrin-brucine conjugated to gold nanoparticles and their application in photodynamic therapy. *Org Biomol Chem* 2010;8:3202-6.
33. Cheng Y, Meyers JD, Broome A-M, Kenney ME, Basilion JP, Burda C. Deep penetration of a PDT drug into tumors by noncovalent drug-gold nanoparticle conjugates. *J Am Chem Soc*. 2011;133:2583-91.
34. Prentice P, Cuschierp A, Dholakia K, Prausnitz M, Campbell P. Membrane disruption by optically controlled microbubble cavitation. *Nat Phys* 2005;1:107-10.
35. Liu HL, Chen WS, Chen JS, Shih TC, Chen YY, Lin WL. Cavitation-enhanced ultrasound thermal therapy by combined low- and high-frequency ultrasound exposure. *Ultrasound Med Biol*. 2006;32:759-67.
36. Arita Y, Torres-Mapa ML, Lee WM, Cizmar T, Campbell P, Gunn-Moore FJ, *et al.* Spatially optimized gene transfection by laser-induced breakdown of optically trapped nanoparticles. *Appl Phys Lett*. 2011;98:093702.
37. Lukianova-Hleb E, Wagner D, Brenner M, Lapotko D. Cell-specific transmembrane injection of molecular cargo with gold nanoparticle-generated transient plasmonic nanobubbles. *Biomaterials*. 2012;33:5441-50.
38. Lukianova-Hleb EY, Ren X, Zasadzinski JA, Wu X, Lapotko D. Plasmonic nanobubbles enhance efficacy and selectivity of chemotherapy against drug-resistant cancer cells. *Adv Mater*. 2012;24:3831-7.
39. Wagner DS, Delk NA, Lukianova-Hleb EY, Hafner JH, Farach-Carson MC, Lapotko DO. The in vivo performance of plasmonic nanobubbles as cell theranostic agents in zebrafish hosting prostate cancer xenografts. *Biomaterials*. 2010;31:7567-74.
40. Lukianova-Hleb E, Belyanin A, Kashinath S, Wu X, Lapotko D. Plasmonic nanobubble-enhanced endosomal escape processes for selective and guided intracellular delivery of chemotherapy to drug-resistant cancer cells. *Biomaterials*. 2012;33:1821-6.
41. Lukianova-Hleb EY, Lapotko DO. Influence of transient environmental photothermal effects on optical scattering by gold nanoparticles. *Nano Lett*. 2009;9:2160-6.
42. Lapotko DO, Lukianova EY, Oraevsky AA. Selective laser nano-thermolysis of human leukemia cells with microbubbles generated around clusters of gold nanoparticles. *Lasers Surg Med*. 2006;38:631-42.
43. Mamot C, Drummond DC, Greiser U, Hong K, Kirpotin DB, *et al.* Epidermal growth factor receptor (EGFR)-targeted immunoliposomes mediate specific and efficient drug delivery to EGFR- and EGFRvIII-overexpressing tumor cells. *Cancer Res*. 2003;63:3154-61.
44. Herbst RS, Langer CJ. Epidermal growth factor receptors as a target for cancer treatment: the emerging role of IMC-C225 in the treatment of lung and head and neck cancers. *Semin Oncol*. 2002;29:27-36.
45. Yokoyama T, Tam J, Kuroda S, Scott AW, Aaron J, Larson T, *et al.* EGFR-targeted hybrid plasmonic magnetic nanoparticles synergistically induce autophagy and apoptosis in non-small cell lung cancer cells. *PLosOne*. 2011;6:e25507.
46. Centocor Ortho Biotech Products. Doxil: Product Information Book. USA: Centocor Ortho Biotech Products. 2011.
47. Jiffar T, Yilmaz T, Lee J, Hanna E, El-Naggar A, Yu D, *et al.* KiSS1 mediates platinum sensitivity and metastasis suppression in head and neck squamous cell carcinoma. *Oncogene*. 2011;30:3163-73.
48. Hleb E, Hafner JH, Myers JN, Hanna EY, Rostro BC, Zhdanok SA, *et al.* LANTCET: elimination of solid tumor cells with photothermal bubbles generated around clusters of gold nanoparticles. *Nanomedicine (Lond)*. 2008;3:647-67.
49. Lapotko DO, Lukianova-Hleb EY, Oraevsky AA. Clusterization of nanoparticles during their interaction with living cells. *Nanomedicine (Lond)*. 2007;2:241-53.
50. Welch AJ, van Gemert MJC. Optical-thermal response of laser-irradiated tissue, 2nd Ed. Springer, 2011.
51. McDannold NJ, Vykhodtseva NI, Hynynen K. Microbubble contrast agent with focused ultrasound to create brain lesions at low power levels: MR imaging and histologic study in rabbits. *Radiology*. 2006;241:95-106.
52. Kennedy JE. High-intensity focused ultrasound in the treatment of solid tumours. *Nat Rev Cancer*. 2005;5:321-7.
53. Rapoport NY, Kennedy AM, Shea JE, Scaife CL, Nam KH. Controlled and targeted tumor chemotherapy by ultrasound-activated nanoemulsions/microbubbles. *J Control Release*. 2009;138:268-76.
54. Ferrara KW. Driving delivery vehicles with ultrasound. *Adv Drug Deliv Rev*. 2008;60:1097-102.
55. Wang CH, Huang YF, Yeh CK. Aptamer-conjugated nanobubbles for targeted ultrasound molecular imaging. *Langmuir*. 2011;27:6971-6.
56. Yin T, Wang P, Zheng R, Zheng B, Cheng D, Zhang X, *et al.* Nanobubbles for enhanced ultrasound imaging of tumors. *Int J Nanomedicine*. 2012;7:895–904.
57. Cavalli R, Bisazza A, Trotta M, Argenziano M, Civra A, *et al.* New chitosan nanobubbles for ultrasound-mediated gene delivery: preparation and in vitro characterization. *Int J Nanomedicine*. 2012;7:3309-18.
58. Cochran MC, Eisenbrey J, Ouma RO, Soulen M, Wheatley MA. Doxorubicin and Paclitaxel loaded microbubbles for ultrasound triggered drug delivery. *Int J Pharm*. 2011;414:161–70.
59. Zhang HF, Maslov K, Stoica G, Wang LV. Functional photoacoustic microscopy for high-resolution and noninvasive in vivo imaging. *Nat Biotechnol*. 2006;24:848-51.
60. Conjusteau A, Ermilov S, Lapotko D, Liao H, Hafner J, Eghtedari M, *et al.* Metallic nanoparticles as optoacoustic contrast agents for medical imaging. *Proc SPIE*. 2006;6086:155-65.
61. Laser Institute of America. American National Standard For Safe Use Of Lasers (ANSI Z136.1–2007). Laser Institute of America. 2007.
62. Lukianova-Hleb EY, Ren X, Constantinou P, Danysh B, Shenefelt D, Carson D, *et al.* Improved cellular specificity of plasmonic nanobubbles versus nanoparticles in heterogeneous cell systems. *PLos One*. 2012;7:e34537.
63. Lukianova-Hleb EY, Oginsky AO, Samaniego AP, Shenefelt DL, Wagner DS, Hafner JH, *et al.* Tunable plasmonic nanoprobes for theranostics of prostate cancer. *Theranostics* 2011;1:3-17.